



LJMU Research Online

Xu, Z, Mei, X, Wang, X, Yue, M, Jin, J, Yang, Y and Li, C

Fault diagnosis of wind turbine bearing using a multi-scale convolutional neural network with bidirectional long short term memory and weighted majority voting for multi-sensors

<http://researchonline.ljmu.ac.uk/id/eprint/20243/>

Article

Citation (please note it is advisable to refer to the publisher's version if you intend to cite from this work)

Xu, Z, Mei, X, Wang, X, Yue, M, Jin, J, Yang, Y and Li, C (2022) Fault diagnosis of wind turbine bearing using a multi-scale convolutional neural network with bidirectional long short term memory and weighted majority voting for multi-sensors. Renewable Energy. 182. pp. 615-626. ISSN 0960-

LJMU has developed [LJMU Research Online](#) for users to access the research output of the University more effectively. Copyright © and Moral Rights for the papers on this site are retained by the individual authors and/or other copyright owners. Users may download and/or print one copy of any article(s) in LJMU Research Online to facilitate their private study or for non-commercial research. You may not engage in further distribution of the material or use it for any profit-making activities or any commercial gain.

The version presented here may differ from the published version or from the version of the record. Please see the repository URL above for details on accessing the published version and note that access may require a subscription.

For more information please contact researchonline@ljmu.ac.uk

<http://researchonline.ljmu.ac.uk/>

1 **Abstract:** In order to solve the problems of insufficient extrapolation of intelligent models for the fault
2 diagnosis of bearings in real wind turbines, this study has developed a multi-scale convolutional neural
3 network with bidirectional long short term memory (MSCNN-BiLSTM) model for improving the
4 generalization abilities under complex working and testing environments. A weighted majority voting rule
5 has been proposed to fuse the information from multi-sensors for improving the extrapolation of
6 multisensory diagnosis. The superiority of the MSCNN-BiLSTM model is examined through experimental
7 data. The results indicate that the MSCNN-BiLSTM model has 97.12% mean F1 score, which is higher
8 than existing advanced methods. Real wind turbine dataset and an experimental dataset are used to to
9 demonstrate the effectiveness of the weighted majority voting rule for multisensory diagnosis. The results
10 present that the diagnosis result of the MSCNN-BiLSTM model with weighted majority voting rule is higher
11 respectively 1.32% and 5.7 % than the model with traditional majority voting or fusion of multisensory
12 information in feature-level.

13 **Keyword:** Bearing; Wind turbine; convolutional neural network; fault diagnosis; information fusion

Nomenclature

MSCNN-BiLSTM	Multi-scale convolutional neural network with bidirection long short term memory
TICNN	Convolution neural networks with training interference
MSCNN-GRU	Multi-scale convolutional neural network with Gate Recurrent Unit
MS-CNN	Multi-scale convolutional neural network
MC-CNN	multi-scale cascade convolutional neural network
CNN	Convolutional neural network
GRU	Gate Recurrent Unit
EMD	Empirical mode decomposition
LSTM	Long short term memory
MCCNN-LSTM	Multi-convolution convolutional neural network with long short term memory
MA-CNN	Multi-head attention convolutional neural network
MSCNN	Multi-scale convolutional neural network
C-CNN	Parallel Convolution Layers with Multi-Scale Kernels
SNR	Signal-Noise-Ratio
WT	Wind turbine
LR	Logistic regression
Conv	Convolutional layer

BN	Batch Normalization
ReLU	Rectified Linear Unit
$y^{l(i,j)}$	the dot product of kernel
W	represents the width of the kernel
$\mathbf{K}_i^l(j')$	the j^{th} weight of kernel l .
$z^{l(i,j)}$	the output of one neuron
μ	the mean of $y^{l(i,j)}$
σ^2	the variance of $y^{l(i,j)}$,
ε	a small constant
$\gamma^{l(i)}$	the scale to be learned
$\beta^{l(i)}$	the shift parameters to be learned
$a^{l(i,j)}$	the activation of $z^{l(i,j)}$
$y_j^s(j)$	the output of the $x(i)$ processed by IMS procedure with the interference
$O_i(k)$	the k^{th} output feature
φ_i	the output of fully connected layer
α_i	The feature weight of each scale
g_t	Input gate
q_t	Output gate
f_t	Forget gate
c_t	Cell state
NREL	National Renewable Energy Laboratory
DAQ	Data Acquisition system

14 1. Introduction

15 Nowadays, various countries have paid more and more attention on the issues about energy security
16 and ecological environment [1].The wind turbines (WT), as one of the most important renewable power
17 productions, are developing rapidly in both terms of installed capacities and sizes because that vigorously

18 developing clean renewable energy has become the universal consensus and concerted action of the
19 international community to promote the transformation of the energy structure and respond to climatic
20 variation [2]. Bearings are the key mechanical parts in a WT's transmission, the health conditions of
21 which determine the power generation efficiency and stable operation of a WT. Therefore, diagnosis and
22 monitoring for bearings in the WTs are necessary for reducing their maintenance costs and delaying
23 service life [3].

24 On the one hand, in benefited from the development of deep learning techniques, a lots of neural
25 network-based methods for maintenance and diagnosis have good graces in the age of digital information
26 industry [4, 5, 6]. In this kinds of neural network-based diagnosis method studies, whether a diagnosis
27 model is developed based on convolutional neural network [7], long short term memory [8] or adversarial
28 network [9], the research points are the structure of network and the construction of data input [10]. But
29 wind-induced vibration of wind turbine leads to complex operating environment of wind turbine [11-12],
30 which leads to become difficulty for neural network-based fault diagnosis model. On the other hand,
31 collaborative maintenance for multisensory diagnosis has become the research hotspot with the advent of
32 the Industry 4.0. Single model performance and information fusion strategy all affect diagnostic results.

33 In order to improve the performance of a diagnostic model, images and raw vibration signals are
34 used as the inputs for training a neural network-based model. Wang *et al.* [13] employed the wavelet
35 spectrogram with a size of 32×32 as the input. The spectrogram, which is based on a 2-D CNN model,
36 was adopted to identify different working states of the rotor systems. In their study, using different sparse
37 convolution neural network increased 5% than using ReLU network. Similarly, Chen *et al.* [14] used the
38 continuous wavelet transform to gain representation images and then imported the images into a 2-D CNN
39 model to address the fault diagnosis. Their model had 99.83% in their test experimental dataset. The
40 difference between their study and Wang's study was that the classifier used in Chen's study is the extreme

41 learning machine, leading to a higher performance under a fault diagnosis task for the rolling bearings.
42 Considering this kinds of input data in the form of images will cause the loss of effective information,
43 Jiang *et al.* [15], using 1-D vibration signals as the input data, proposed a diagnosis model based on the
44 multi-scale convolutional neural network (MS-CNN) to diagnose gearbox faults of a wind turbine. The
45 results indicated that the time scale of the MS-CNN model has a significant impact on the diagnosis effect
46 of the model and got 98.53% on their experimental dataset. Zhao *et al.* [16] used 1-D vibration signal as
47 the input of the proposed normalized CNN for an intelligent fault diagnosis of rolling bearings. The results
48 show that the normalized CNN model has a better extrapolation ability by 98.50% than a traditional CNN
49 model. Wang *et al.* [17] used 1-D CNN-based network to examine ten groups of bearings to validate its
50 reliability. The results showed that the diagnostic performance of the model under variable conditions
51 was improved to 99.93% because more fault information was considered. Wei *et al.* [18] adopted 1-D raw
52 vibration signals of rolling bearing as the input of a deep CNN to simultaneously achieve feature
53 extraction and classification. Huang *et al.* [19] convoluted the 1-D vibration signals by different kernel
54 sizes to obtain different resolutions in frequency domain, which was introduced in to a CNN-based model
55 to develop a multi-scale CNN diagnosis model to address the fault identification of bearings, which had
56 83.2% diagnosis result on their experimental dataset. Considering the contents of the fault information,
57 Zhao *et al.* [20] proposed a bi-directional LSTM framework to monitor machine health. Lu *et al.* [21]
58 used the LSTM with the deep neural network to address fault diagnosis at the beginning of failures. In
59 summary, using raw vibration signals as the data set to train a neural network-based model for fault
60 diagnosis are more robust than using images. Considering multi-scale information and the potential
61 semantics relationships of fault information are helpful to improve a model's extrapolation performance.
62 Therefore, combining the advantages of the above studies for establishing a single sensor model, the first
63 motivation in this paper is to design the Multi-Scale CNNBiLSTM network for considering both multi-

64 scale information capability and context association of fault information.

65 In the studies of multisensory information fusion strategies to machine diagnosis for collaborative
66 maintenance, Jing et al. [22] and Azamfar et al [23] directly fused raw signals from multiple sensors as a
67 multi-signals and used a CNN to extract advanced features for gearbox fault diagnosis. The above studies
68 are based on the signal fusion level to process the information collected by multiple sensors. Although
69 there are little loss through the date-level fusion, big data and noisy make those are not easy to achieve
70 truly engineering. As an alternative, Chen et al. [24] and Liu et al. [25] first constructed a multi-sensor
71 features then realize information fusion in the feature-level to finally diagnose fault. However, those kinds
72 of feature fusions in the feature-level have better interpretabilities when facing the same category of
73 information fusion. If the advanced features are derived from different information sources, the
74 interpretability will be not strong enough. Therefore, the realization of information fusion in the decision-
75 making level is a relatively suitable choice to address multi-sensor fault diagnosis for wind turbine
76 maintenance [26]. Therefore, the second motivation in this paper is to design a weighted voting rule based
77 on Genetic Algorithm (GA) for multisensory fault diagnosis. The disadvantages of CNN-based fault
78 model, RNN-based model and multi-sensor fault diagnosis method are summarized in Table 1.

Table 1: Brief compared of diagnosis method

Methods	Advantages	Disadvantages	References
CNN-based model	End-to-end feature extraction Fast calculation	Ignoring the temporal correlation of fault features	15, 19, 40, 41, 42
RNN-based model	Considering the semantics of the fault features	Large amount of calculation	38
CNN-RNN-based model	End-to-end feature extraction Considering the semantics of the advanced fault features	Single feature extraction The order of advanced features is not considered	39, 43
Multisensory diagnosis	Consider multiple sources of information	Strategy of information fusion is not considered	36, 30

79 In order to improve the generalization abilities of a neural network-based model for fault diagnosis
80 and fusing the diagnostic results from multiple sensors in a suitable way to increase the final diagnostic

81 accuracies and robustness for wind turbine bearing maintenance. The Multi-Scale CNNBiLSTM model,
82 based on multi-scale coarse-grained procedure algorithm, convolutional neural network and Bidirectional
83 long short memory network, has been developed in this paper to capture multi-scale time information and
84 associate fault semantic information. A weighted majority voting method based on Genetic Algorithm is
85 proposed to fuse the diagnostic results corresponding to every sensor for improving robustness of the
86 diagnostic method. The proposed Multi-Scale CNNBiLSTM model is examined through comparison with
87 experimental data of noise and variable loading scenarios to verify its reliability and superiority in real
88 wind turbine. The originalities and main contributions of this study are summarized as follows.

89 (1) The Multi-Scale CNNBiLSTM model, based on multi-scale coarse-grained procedure algorithm,
90 convolutional neural network and Bidirectional long short memory network, has been developed in this
91 paper to capture multi-scale time information and associate fault semantic information for improving the
92 performance of a single model.

93 (2) An end-to-end intelligent diagnosis framework based on the Multi-Scale CNNBiLSTM model is
94 developed to realize fault diagnosis of a rolling bearing, which is capable of directly operating on the
95 measured raw signals without any manual modifications.

96 (3) A weighted majority voting method based on genetic algorithm has been proposed to fuse the
97 diagnostic results of different sensors in decision-making level, which has better information fusion
98 interpretation.

99 The remaining parts of the paper are organized as follows. The development of the Multi-Scale
100 CNNBiLSTM framework is presented in Section 2. The experimental data of a test experimental data and
101 the evaluation index is presented in Section 3. The validation and discussion of the Multi-Scale
102 CNNBiLSTM model under various working conditions are presented in Section 4. Conclusions are
103 presented in Section 5.

104 2. Methodologies about Multi-Scale CNNBiLSTM

105 2.1 Multi-scale extraction

106 A multi-scale coarse-grained process has been developed and implemented into a multi-scale feature
 107 extraction layer to extract more information from raw signals with multiple time scales [15]. However,
 108 the multi-scale layer in reference [15] adopted the non-continuous sampling when capturing the multi-
 109 scale information, which leads to omission of some inherent information.

110 The processing for calculating the traditional multi-scale coarse-grained procedure, is based on a
 111 given time series, $x_i : 1 \leq i \leq n$ and the coarse-grained time series as the time scale factor of τ in order
 112 to calculate a sub-signal y_j^τ through Eq. (1).

$$y_j^\tau = \frac{1}{\tau} \sum_{i=(j-1)\tau+1}^{j\tau} x_i, 1 \leq j \leq (n/\tau) \quad (1)$$

113 where $\tau = 1, 2, 3, \dots$ is the time scale factor. The length of the sub-signal y_j^τ is (n/τ) .

114 An illustration of the traditional multi-scale operation for a time scale factor $\tau=3$ is presented in
 115 Figure 1.

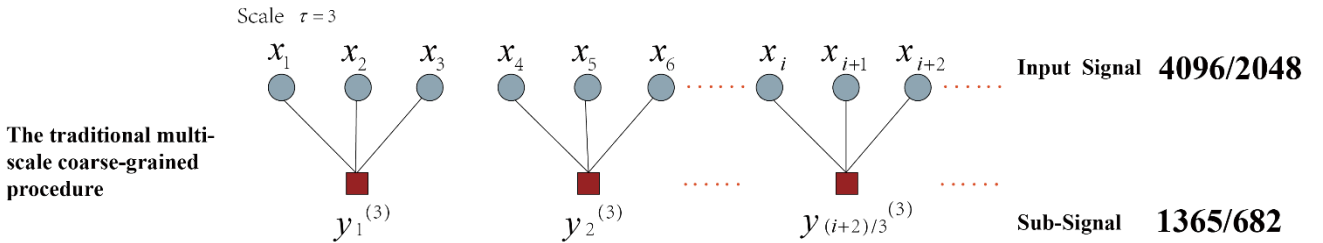


Figure 1: The traditional multi-scale coarse-grained operation

116 As shown in Figure 1, the length of the sub-signal decreases exponentially with increase in the time
 117 scale factor, which leads to its inability to perform the convolution process in a very deep convolution
 118 layer. More importantly, some useful information of the fault representation will not be captured due to
 119 discontinuity in the operation of a traditional MS coarse-grained procedure.

120 In order to solve the shortcomings of the traditional MS operation, a novel multi-scale coarse-grained
 121 procedure is developed and presented in this section. Figure 2 shows the continuous multi-scale coarse-

122 grained procedure when the time scale factor τ is 3. The sub-signal z_j^n obtained by the CMS operation
 123 at any time scale factor τ is calculated by Eq (2).

$$z_j^{n-\tau} = \begin{cases} \frac{1}{\tau} \sum_{i=(j-1)+1}^{(j-1)+1+\tau} x(i), & j \in [1, n-\tau], \tau \geq 2, z_{n-\tau}^n = \mathbf{0}, j \in [n-\tau, n] \end{cases} \quad (2)$$

124 where $\tau = 1, 2, 3, \dots$ is the time scale factor. The length of the sub-signal z_j^n is n .

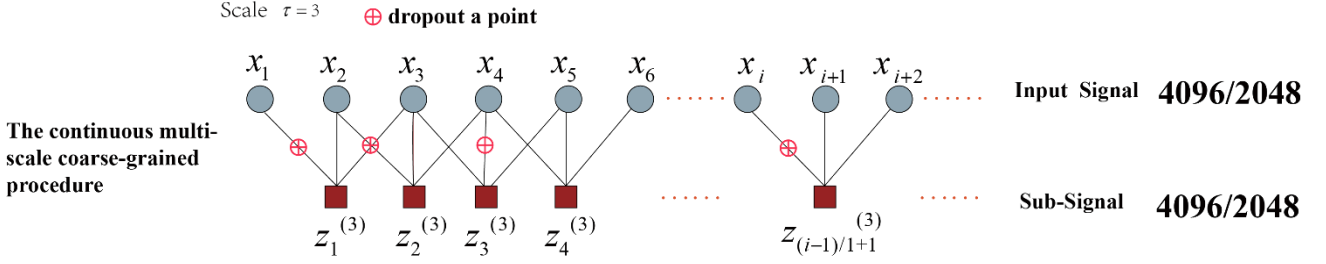


Figure 2: The continuous multi-scale coarse-grained operation

125 Compared with Figure 1, the length of the sub-signal processed by the CMS procedure will not
 126 decrease with time scale factor τ , which makes the CMS-based model easier to be maintained. In
 127 addition, some data points are randomly discarded using the dropout technology in the coarse-grained
 128 extraction process, in order to avoid the overfitting of data when training a model and to improve its
 129 robustness. Thus, the output z is given by Eq. (3).

$$\begin{cases} p \sim Uniform(0.1 \sim 0.2) \\ r_i^1(k) \sim Bernoulli(p) \\ z_j^\tau(j) = r_i^1 \cdot K_i^1 \cdot x_i \end{cases} \quad (3)$$

130 where (\cdot) represents the element-wise product, when the dropout rate p obeys the uniform distribution
 131 $U(0.1, 0.2)$; $r_i^1(k)$ follows the Bernoulli distribution, which is used to determine whether the k^{th} element
 132 in the i^{th} frame of the convolutional K_i^1 is dropped or not. $z_j^\tau(j)$ is the output of x_i processed by the
 133 CMS procedure with an interference in every batch training.

134 2.2 Feature learning layer

135 The feature learning layer consists of parallels of 1D CNNs that extract representation features from
 136 the sub-signals. Generally, a CNN structure is mainly composed of various pairs of convolutional layers
 137 and pooling layers. The activation function is used to realize the linear separation of the high-dimensional

138 features after the convolution operations. \mathbf{K}_i^l is the i^{th} filter in layer l , and $\mathbf{X}^{l(\mathbf{R}^j)}$ is j^{th} local area in
 139 the convolutional layer l . The convolutional process is given as follows:

$$y^{l(i,j)} = \mathbf{K}_i^l \cdot \mathbf{X}^{l(\mathbf{R}^j)} = \sum_{j'=0}^W \mathbf{K}_i^l(j') \mathbf{X}^{l(j+j')} \quad (4)$$

140 where $y^{l(i,j)}$ denotes the dot product of kernel and the local area. W represents the width of the kernel.
 141 $\mathbf{K}_i^l(j')$ is the j^{th} weight of kernel l .

142 In order to enhance the non-linear expression ability of the input signal and to more easily identify
 143 the learned features, the ReLU activation function is added after the convolutional layer. The formula for
 144 the ReLU is given in Eq. (8):

$$a^{l(i,j)} = f(z^{l(i,j)}) = \max\{0, z^{l(i,j)}\} \quad (5)$$

145 where $z^{l(i,j)}$ is the output array of the Batch Normalization (BN) and $a^{l(i,j)}$ is the activation of $z^{l(i,j)}$.

146 In order to efficiently accelerate the network training and to avoid the problem of gradient
 147 disappearance caused by activation function, the BN technique is introduced before the pooling operation.
 148 The n -dimensional array $\mathbf{y}^l = (y^{l(1)}, y^{l(2)}, \dots, y^{l(n)})$ to the l^{th} BN layer is represented as
 149 $\mathbf{y}^{l(i)} = (y^{l(i,1)}, y^{l(i,2)}, \dots, y^{l(i,n)})$ and $\mathbf{y}^{l(i)} = y^{l(i)} = y^{l(i,1)}$ when the BN layer is placed after the convolutional
 150 layer and fully connected layer, respectively. The formula for the BN operation is presented as follows:

$$\hat{y}^{l(i,j)} = \frac{y^{l(i,j)} - \mu}{\sqrt{\sigma^2 + \varepsilon}}, z^{l(i,j)} = \gamma^{l(i)} \hat{y}^{l(i,j)} + \beta^{l(i)} \quad (6)$$

$$\mu = \frac{1}{n} \sum_{i=1}^n y^{l(i,j)} \quad (7)$$

$$\sigma^2 = \frac{1}{n} \sum_{i=1}^n (y^{l(i,j)} - \mu)^2 \quad (8)$$

151 where $z^{l(i,j)}$ is the output of one neuron. μ and σ^2 are the mean and variance of $y^{l(i,j)}$, respectively.

152 ε is a small constant introduced to prevent the calculation from being invalid when the variance is 0.

153 $\gamma^{l(i)}$ and $\beta^{l(i)}$ are respectively the scale and shift parameters to be learned.

154 The pooling layer is also called the down-sampling layer. The most common pooling techniques
 155 include average pooling and maximum pooling. The maximum pooling is chosen in this research, and it
 156 is presented in Eq (9).

$$p^{l(i,j)} = \max_{(j-1)W+1 \leq t \leq jW} \{a^{l(i,t)}\} \quad (9)$$

157 where $a^{l(i,t)}$ is the value of the t^{th} neuron in the i^{th} framework of layer l ; W is the width of
 158 pooling size; $p^{l(i,j)}$ is the corresponding value of the neuron in layer l of the pooling, and
 159 $t \in [(j-1)W+1, jW]$.

160 **2.3 The BiLSTM layer**

161 The LSTM, proposed by Hochreiter *et al.* [27], is a variant of the Recurrent Neural Network (RNN).
 162 Using a standard RNN model [28] to calculate a given sequence $z_m = (z_1, z_2, z_3, \dots, z_m)$ that is obtained
 163 by the CMSCNN layer for obtaining a hidden sequence $h = (h_1, h_2, \dots, h_m)$ and an output sequence
 164 $Z_m = (Z_1, Z_2, \dots, Z_m)$. In order to overcome the shortcoming of the LSTM, thus in this study, BiLSTM is
 165 used to consider the semantic relevance of the information from both of the forward and backward of
 166 advanced features, which are represented as Eq. (10). The forward and backward information are fused
 167 into the fully connected layer and softmax function to calculate the probabilities of each failure.

$$Z = [Z_f, Z_b] \quad (10)$$

168 Where Z_f is the forward features; Z_b is the backward features.

169 The forward and backward features calculations are similarity. Take the forward features as an
 170 example, the calculation of Z_f is shown below, which also is the LSTM.

$$h_t = f_a(W_{zh}x_t + W_{hh}h_{t-1} + b_h) \quad (11)$$

$$Z_t = W_{zh}h_t + b_z \quad (12)$$

171 where W represents the weight coefficient matrix; b is the offset vector; f_a is the activation function;

172 The subscripts t represents time.

173 The LSTM network is proposed to solve the problems of the gradient disappearance and gradient
 174 explosion, which owns long-term memory. The input gate g_t , output gate q_t , forget gate f_t and cell
 175 activation vector C_t are updated in the LSTM. The LSTM cell structure in a hidden layer is presented
 176 in Figure 3.

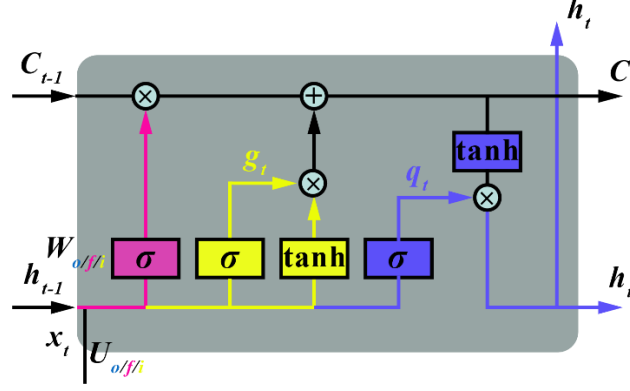


Figure 3: The LSTM structure

177 The updating equations are given as follows:

$$g_t = \sigma(\sum U_g x_t + \sum W_g h_{t-1} + b_g) \quad (13)$$

$$f_t = \sigma(\sum U_f x_t + \sum W_f h_{t-1} + b_f) \quad (14)$$

$$q_t = \sigma(\sum U_o x_t + \sum W_o h_{t-1} + b_o) \quad (15)$$

$$C_t = f_t C_{t-1} + g_t \tanh(\sum U_i x_t + \sum W_i h_{t-1} + b_i) \quad (16)$$

$$h_t = q_t \tanh(C_t) \quad (17)$$

178 where g_t , q_t , f_t and c_t are the input gate, output gate, forget gate and cell state respectively; W
 179 and b are the corresponding weight coefficient matrix and bias term, respectively; σ and \tanh are
 180 the sigmoid and hyperbolic tangent activation functions, respectively.

181 2.4 Classification layer

182 The probability distributions of the representative features extracted by the 1-D CNN and BiLSTM
 183 layer, are fed into the fully connected layer for classification. Each output is mapped into a probability by
 184 a softmax function φ , which is defined by

$$\varphi(u_c) = \frac{e^{u_c}}{\sum_{c=1}^T e^{u_c}}, c = 1, 2, \dots, T \quad (18)$$

185 where $\varphi(u_c)$ is a T -dimensional probability vector and denotes the probability distribution under T kinds
 186 of test scenarios, u_c is the fusion features.

187 2.5 The proposed Multi-Scale CNNBiLSTM architecture

188 The proposed Multi-Scale CNNBiLSTM architecture consists of the multi-scale layer, the feature
 189 learning layer consisted of 1-D CNN, the BiLSTM layer and the classification layer. Figure 4 presents
 190 the proposed MSCNN-BiLSTM framework.

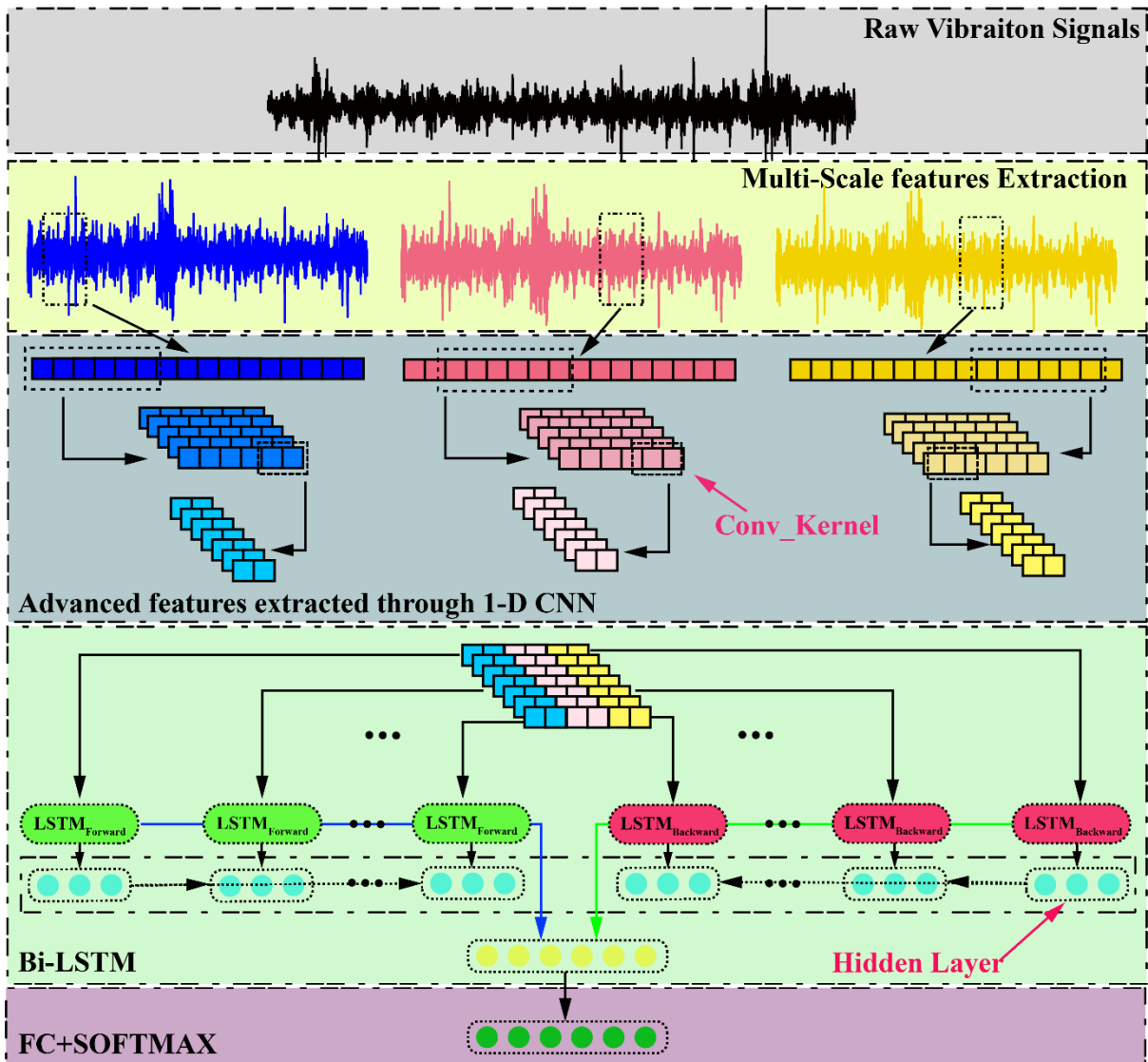


Figure 4: The architecture of the CMSCNN-LSTM model

191 As shown in Figure 4, the vibration signals measured by a sensor are fed into the MSCNN-BiLSTM
 192 network. The representation features with lower dimension features are obtained by the multi-scale layer

193 and multiple parallels of 1-D CNN. The number of time steps of the advanced features fed into the
 194 BiLSTM network is decreased significantly from n to L , where n is the length of the input sequences, and
 195 L is the number of elements in the pooling layer. The relevant information is obtained by BiLSTM, which
 196 hidden in each advanced features of the forward and backward are fused into fully connected layer to
 197 calculate the probabilities of each working condition.

198 In contrast to the CNN-based model and LSTM-based model, the advantage offered by the structure
 199 of the proposed MSCNN-BiLSTM model is that its capability of examining time multi-scale features,
 200 which can capture more information needed to improve the performance of the model. The problem of
 201 high time complexity caused by being fully connected with the LSTM network has been improved by
 202 implementation of the pre-processing capability within using the advanced features as the feature vectors
 203 of a RNN network.

204 The improvement of the multi-scale coarse-grained procedure makes the data length of the sub-
 205 signals that obtained by the improved MS layer are the same as the original inputs. Which makes the
 206 feature extraction procedure using a CNN model to be more uniform and easier to be modified and
 207 maintained. The parameters of the feature extraction layer based on the 1D CNN in Figure 4 are presented
 208 in Table 2.

Table 2: The details of the 1D CNN in the CMSCNN-LSTM model

No.	Layers	Kernel Size/Stride	Filter numbers	Outputs Size
1	A sub-signal	-	-	[4096,1]
2	Conv_1	[128,1]/[5,1]	16	[794,1]
3	Pool_1	[64,1]/[3,1]	16	[395,1]
4	Conv_2	[2,1]/[2,1]	32	[111,1]
5	Pool_2	[3,1]/[2,1]	32	[54,1]
6	Conv_3	[2,1]/[1,1]	8	[18,1]
7	Pool_3	[3,1]/[2,1]	8	[7,1]

209 The parameters of the 1D CNN in the MSCNN-BiLSTM model are shown in details in Table 2.

210 Compared with the CNN structure in other studies, the number of filters increases with the layers

211 deepening. However, the number of filters of the last convolution layer is too small to reduce the time
212 complexity. The BN layer and the ReLU activation are introduced between the convolution layer and the
213 pooling layer to prevent the gradient disappearing.

214 The MSCNN-BiLSTM model is optimized by the Adam gradient descent optimization algorithm
215 with a mini-batch size of 256 samples. The loss function is cross entropy. The learning rate is initialized
216 to 0.001 with no decay on each update. A dropout layer is added before the fully connected layer to
217 minimize over-fitting risk.

218 ***2.6 Weighted majority voting for multisensory diagnosis***

219 It can be seen from review studies that the multisensory intelligent fault diagnosis is not only affected
220 by the performance of a model [29], but how to summarize the useful information from multiple sensors
221 also has significant impact on the final diagnostic results [30]. As a single model, the proposed MSCNN-
222 BiLSTM has good performance. Therefore, in this study, motivated from the ensemble learning. Each
223 MSCNN-BiLSTM model is regarded as a sub-model. Using different signals acquiring from different
224 sensors as dataset to train MSCNN-BiLSTM model will integrate multiple learners to develop an
225 improved deep learner to work in tandem. The weighted majority voting rule treats the predictions as the
226 final class label. The choice of weights directly affects the final diagnostic result. Eq. (19) delineates
227 weighted majority voting.

$$H(x) = C_{\text{armax}_j} \sum_{n=1}^N w_n h_n^j(x) \quad (19)$$

228 Where for each probabilities x , the prediction of N sub-model is $h_n^j(x)$. The weighted for majority voting
229 of each $h_n^j(x)$ is w_n . The final prediction labels $H(x)$ is calculated by the $C_{\text{armax}_j}(\cdot)$ to find out which
230 prediction has the most votes.

231 Weights play a key role in weighted majority voting rule. Thus, in this paper, GA [31] is used to find
232 the optimized weights for majority voting. The motivation of using GA to evaluate weights is that we

233 hope the weights can help to improve the F1 score of the ensemble MSCNN-BiLSTM framework. The
 234 fitness functions of the GA consist of F1 score. Assumed the MSCNN-BiLSTM model will solve a k-
 235 classification problem, the weights are $w_n^k = [w_n^1, w_n^2, \dots, w_n^k]^T$. The pseudo-code to solve the weight of the
 236 weighted majority vote is shown in Table 3

Table 3: Pseudo-code of weighted majority voting rule

Input: the output probabilities of each MSCNN-BiLSTM

Initial: initialization of the GA parameters, including N_{pop} , Proportion of cross variation (P_c, P_m) and the maximum iteration N_{max}
 Based on N_{pop} to Initialize the population and reset the number of iterations as $n = 1$

while $n \leq N_{\text{max}}$ **perform**

Through the $w_n^k = [w_n^1, w_n^2, \dots, w_n^k]^T$ to calculate the weighted voting for each sensor

Calculate fitness through the F1 score

Choose according to competitive strategy

Perform crossover and mutation and renew the population

Determine convergence

if convergence **then**

jump out of the loop

end

end

end: Output the best weights for weighted majority voting

237 **2.7 Fault diagnosis framework based on the MSCNN-BiLSTM for multisensory**

238 In the section, the proposed MSCNN-BiLSTM model is examined using experiments on a bearing
 239 test rig. Figure 5 presents the fault diagnosis workflow based on the MSCNN-BiLSTM for multisensory.

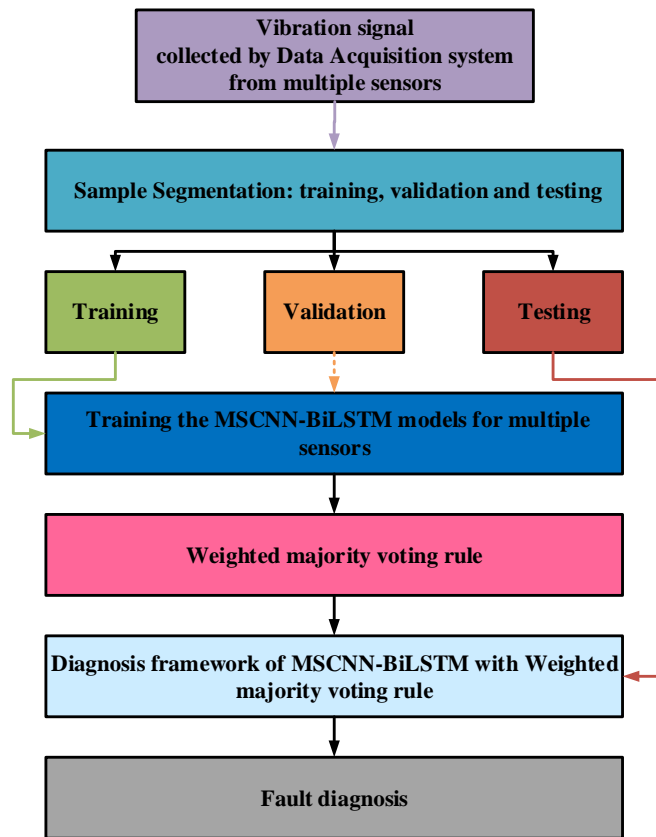


Figure 5: The fault diagnosis system based on the MSCNN-BiLSTM model with weighted majority voting rule

240 Figure 5 presents the intelligent diagnosis flowchart of wind turbine bearing based on MSCNN-
 241 BiLSTM model for multisensory. Using data acquisition system to obtain vibration signals from different
 242 sensors. Training dataset and validation dataset are built through sample segmentation and standardization.
 243 The best parameters of the MSCNN-BiLSTM model are trained and saved by cross validation. The
 244 number of the MSCNN-BiLSTM models are determined by the number of the sensors. For instance, use
 245 two sensors to collect signals can be used to train two MSCNN-BiLSTM models with different parameters.
 246 In order to integrate each MSCNN-BiLSTM model's performance, same as the ensemble learning, the
 247 predictions of the multiple MSCNN-BiLSTM models are fused in decision-making level through the
 248 proposed weighted majority voting rule for multisensory diagnosis.

249

250 **3. Experiments and evaluation method**

251 *3.1 The description of experiment datasets*

252 The bearing experimental data from Case Western Reserve University (CWRU) [32] and XJTU
253 Xi'an Jiao Tong University (XJTU) [33] is used to construct different test scenarios to examine the
254 performance of the proposed MSCNN-BiLSTM method. The NREL wind turbine transmission database
255 is used to examine the practical application abilities in engineering of the proposed multisensory diagnosis
256 method [34].

257 The CWRU experimental data, as the standard bearing vibration data set, is used to examine the
258 performances of three kinds of RNN variants that include LSTM, BiLSTM and GRU and to compare the
259 performance with CNN-based models for proving the superiority of the MSCNN-BiLSTM model. The
260 data of CWRU covering normal state, inner race fault, ball fault and outer race fault in different azimuths
261 (3, 6 and 12 o'clock directions) are selected by two sensors with different sampling frequencies in order
262 to validate the developed MSCNN-BiLSTM model. The data is examined for each of the fault category
263 stated above. In total, 11 sets of data are used in this study. The motor loads range from 0 HP to 3 HP and
264 the tested bearing model is SKF 6205.

265 The experimental data of CWRU is used to build different scenario and it is presented in Table 4.

Table 4: Datasets of bearing fault diagnosis for variable loads test

Datasets labels	Samples	Number of samples	Loads (hp)
I	Training	1600	0,1,2,3
	Test	160	0,1,2,3
II	Training	1600	0,1,2,3
	Test	160 (Added noise)	0,1,2,3

266 The data of XJTU covering inner race fault, cage fault outer race fault, and hybrid faults that consist
267 of inner race, ball, cage and outer race failure, is selected by two sensors with different sampling directions
268 to validate the developed MSCNN-BiLSTM model when the failures are weak. In the XJTU data includes

269 the full-life of a bearing, the extrapolation abilities of the MSCNN-BiLSTM model are examination
 270 through the manually segmentation samples set that contain different damage magnitudes. Table 5
 271 presents the details of the scenario setting for bearing degradation adaptation. The normal distribution of
 272 inner race fault from Phase 1 to Phase 3 are presented in Figure 6.

Table 5 Details of the bearing degradation configuration

Case Name	Training samples	Testing samples
A	Phase 1	Phase 2
B	Phase 1	Phase 3
C	Phase 2	Phase 1
D	Phase 2	Phase 3
E	Phase 3	Phase 1
F	Phase 3	Phase 2

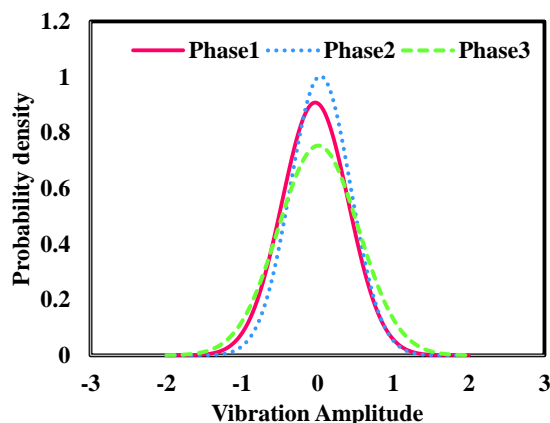
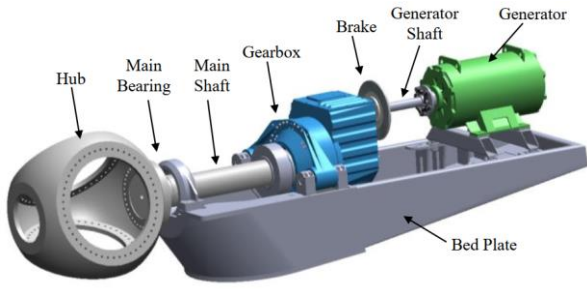


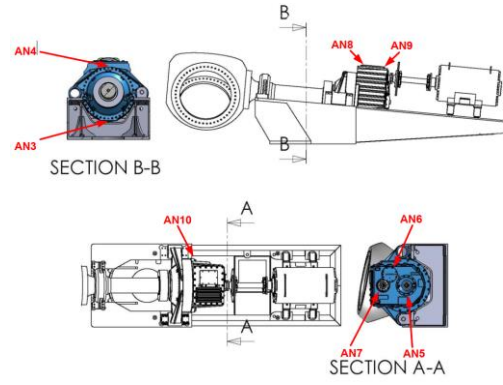
Figure 6: The normal distribution of different phases

273 As shown in Table 5 and Figure 6, six scenarios are constructed by extracting data from three
 274 different stages in the XJTU experimental process of bearing degradation. Phase 1, Phase 2 and Phase 3
 275 respectively represent the development process of bearing failures from small to large, but it is worth
 276 noting that the data of the complete failure phase is not selected. The probability densities of the normal
 277 distributions of the three phases are different. Therefore, the bearing damage magnitude adaptation
 278 scenario test is used to verify the effectiveness of the proposed method.

279 Wind turbine condition monitoring benchmarking dataset provided by National Renewable Energy
 280 Laboratory is used to examine the proposed MSCNN-BiLSTM in the real engineering. The test turbine
 281 drive train configuration and the vibration sensor locations on wind turbine are shown in Figure 7 [35].



(a) Wind turbine drive train configuration



(b) Vibration sensor locations

Figure 7 The illustration of the NREL test wind turbine

282 Table 6 presents a compiled list of the actual damage occurred to the test drive train system. The
 283 damage detection are deemed through vibration analysis. In this study, HS-SH downwind bearing
 284 overheating, IMS-SH assembly damage of upwind and downwind bearings are used to build dataset for
 285 training MSCNN-BiLSTM model.

Table 6: Datasets of damage bearings of NREL wind turbine

labels	Samples	Number of samples	Sensors	Mode
1	Training	200	AN8	Healthy condition 1
	Test	200	AN9	
2	Training	200	AN5	Healthy condition 2
	Test	200	AN6	
3	Training	200	AN8	HS-SH downwind bearing overheating
	Test	200	AN9	
4	Training	200	AN5	IMS-SH downwind bearings damage
	Test	200	AN6	

286 3.2 Development environment and evaluation methodology

287 Different scenarios created based on the four aforementioned datasets are used to examine the
 288 proposed MSCNN-BiLSTM model. The data mining and setup of the deep learning model is conducted
 289 using the MATLAB[®] Deep Network Designer, MATLAB version 9.70 (R2019b, The MathWorks, Inc.,
 290 Natick, MA, USA).

291 The F1 score is used to evaluate and compare the performance of the diagnosis model examined in
 292 this study, which offers a comprehensive metric to measure the extrapolation of the model. The definition
 293 of the F1 is presented in Eq. (20).

$$F1 = \frac{2TP}{2TP + FP + FN} \quad (20)$$

294 where TP, FP, TN and FN mean correctly classified as positive samples, misclassified as positive samples,
 295 correctly classified as negative samples and misclassified as negative samples, respectively.

296 4. Validation and discussion

297 4.1 Comparison of the RNN variants

298 The LSTM module of the MSCNN-BiLSTM model is used to consider the long-term dependences
 299 of fault information. In this section, the influence of type of the RNN networks including the LSTM,
 300 BiLSTM [36] and GRU [37] is investigated using dataset II when integrated with the MSCNN model.
 301 The diagnosis models are named as MSCNN-LSTM and MSCNN-GRU. Figure 8(a) and Figure (b) show
 302 the accuracy and loss curves of training and validation of the three models. Figure 8 (c) presents the
 303 performance of the models examined using dataset II with SNR from -4dB to 4dB. Table 7 gives the
 304 training time, response time and F1 score of the methods examined in -4dB.

Table 7: Comparison of the performances of the MSCNN-LSTM model, the MSCNN-BiLSTM model and the MSCNN-GRU model

Methods	F1 score (%)	Training time (s)	Testing time (s)
MSCNN-LSTM	85.58±0.29	206.84+16.57	0.4943±0.0037
MSCNN-BiLSTM	86.93±0.17	209.85+19.45	0.4557±0.0035
MSCNN-GRU	86.83±0.21	204.42+16.93	0.4789±0.0038

305

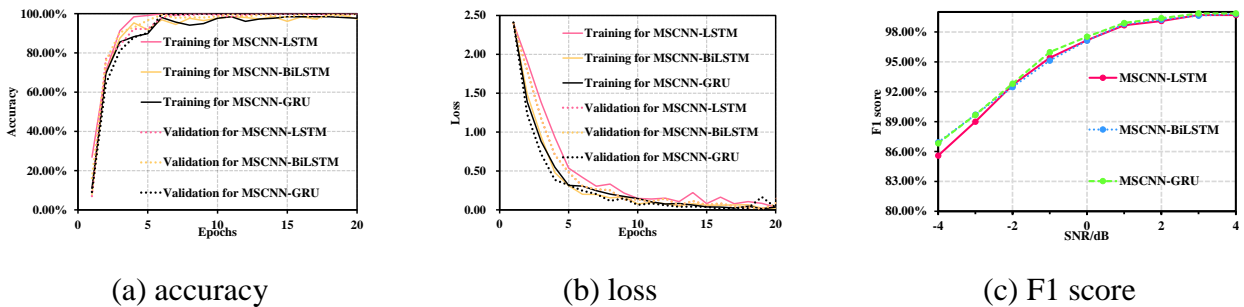


Figure 8: The training and validation accuracy curves of the three models with increasing epochs and performances of the models examined using dataset II with SNR from -4dB to 4dB.

306 Figure 8 (b) presents the loss curves of the models' training and validation. The loss of the MSCNN-
 307 LSTM is the most unstable model among the three RNN-variants model, while the MSCNN-BiLSTM

308 model is stable due to the fusion of forward and backward information. As shown in Table 4 and Figure
309 8, the differences between the training/response times of the variants are insignificant. The MSCNN-
310 BiLSTM has a slightly longer training time and a shorter response time. That is because forward and
311 backward propagation of advanced features to record different fault context information. It is noted that
312 the MSCNN-GRU model examined in the 0 dB environment has the highest F1 score of 97.5%. This is
313 because the GRU only contains update and reset gates. However, in a noisy environment (-4dB), the
314 MSCNN-BiLSTM model has the highest F1 score of 86.9%, which is because the LSTM units can control
315 whether the important information in them is retained or not. The two-way propagation makes the
316 BiLSTM unit more capable of capturing long-term dependencies, which gives the model a better noise
317 immunity. Thus, the MSCNN-BiLSTM model performs better in a large noise environment, which also
318 proves the motivation of the proposed MSCNN-BiLSTM model.

319 ***4.2 Comparison with advanced methods***

320 In order to confirm the superiority of the MSCNN-BiLSTM model in identifying the failure types
321 and the failure magnitudes of the bearings in the noisy environments, Figure 10 provides the comparisons
322 of the proposed MSCNN-BiLSTM, the LSTM [38], the CNN-LSTM [39], TICNN [40], MC-CNN [19],
323 C-CNN [41], MA-CNN[42], MCCNN-LSTM[43], and MS-CNN [15] by using average F1 scores with
324 10 trails examined on dataset H with -4dB noise level to 4dB noise level. The diagnosis results of nine
325 methods under different noise environments are shown in Figure 9 to further demonstrate the reliability
326 of the proposed MSCNN-BiLSTM model. Table 8 presents the details of the F1 scores in average, nine
327 methods examined by dataset II with 0 dB in 10 trails.

Methods	F1 score (%)
MSCNN-BiLSTM [Our method]	97.12 ±0.09
CNN-LSTM [2020]	92.03 ±0.24
MS-CNN [2019]	83.75 ±0.78

LSTM [2019]	83.08±1.49
TICNN [2018]	82.23±0.92
MC-CNN [2019]	81.19±1.92
C-CNN [2020]	75.83±1.14
MA-CNN [2020]	67.15±1.43
MCCNN-LSTM [2021]	96.00±0.15

328

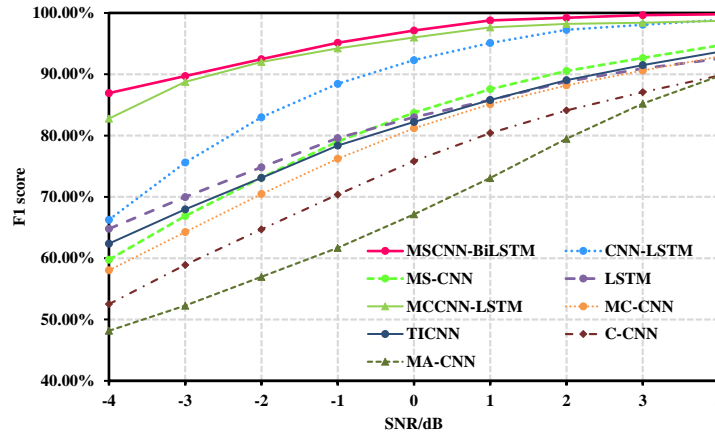


Figure 9: Diagnosis results examined in 10 trails on the noisy signals with different SNRs

329

As shown in Figure 9, the proposed MSCNN-BiLSTM model always shows the highest average F1

330

score with the SNR changed from -4dB to 4dB. The performance of the MCCNN-LSTM model is second

331

only to the MSCNN-BiLSTM model. There are two possible reasons why the MSCNN-BiLSTM is better

332

than the MCCNN-LSTM: 1. the multi-scale features extraction of the MSCNN-BiLSTM is developed

333

based on multi-scale coarse-grained algorithm, which is more robust than the MCCNN-LSTM model

334

using multi-scale convolution to extract multi-scale information. 2. The proposed MSCNN-BiLSTM

335

considers the forward and backward fault semantics, which can capture more useful information than the

336

MCCNN-LSTM only consider single direction fault semantics. Besides, The MA-CNN performs poorly

337

when the test date source contains noise. That is because, the MA-CNN is used the gray images of the

338

vibration signals as the inputs of the CNN-based model.

339

4.3 Damage magnitude detection adaptation scenario test for multisensory

340

In the damage magnitude detection adaptation scenario, the training dataset and the test dataset are

341

from a same data source but diatribe differently due to the damage evolution, which can prove a strong

342 extrapolation the proposed MSCNN-BiLSTM model has. Table 9 give the weights of majority voting and
 343 F1 score of each sensor.

Table 9: The weights of majority voting and F1 score for every conditions and sensor

	Weights for majority voting [Sensor1, Sensor2]	F1 Score (Sensor 1/ Sensor 2/ Fusion)
Inner Race fault	[1, 1]	(0.9887/0.9962/ 0.9963)
Cage fault	[1, 2]	(0.9197/0.9876/ 1.0000)
Outer race fault	[1, 1]	(0.8503/1.0000/ 1.0000)
Hybrids faults	[1, 2]	(0.9975/1.0000/ 1.0000)

344 As shown in Table 9, the examined results of MSCNN-BiLSTM model show that there are low F1
 345 scores of the cage fault and outer rave fault for each sensor due to damage evolution and added noise
 346 (SNR=-4). Although the mean of F1 score of each sensor is high, there is a little false alarm rate that is
 347 needed to be avoided in fault diagnosis. The proposed weighted majority voting can integrate the positives
 348 of each sensor, through the weights votes, to improve F1 score of each classified conditions. It can be
 349 seen that the F1 score of cage fault for sensor 1 increases from 0.9197 to 1.0000, the F1 score of outer
 350 race fault for sensor 1 increases from 0.8503 to 1.0000. To further explain the mechanism of the weighted
 351 majority voting rule, confusion matrix is used to show how the weighted voting majority rule to improve
 352 the performance of the MSCNN-BiLSTM model for multisensory diagnosis. Figure 10 presents the
 353 diagnosis results, tested in different damage magnitude to examine the extrapolation of the MSCNN-
 354 BiLSTM model for multisensory.

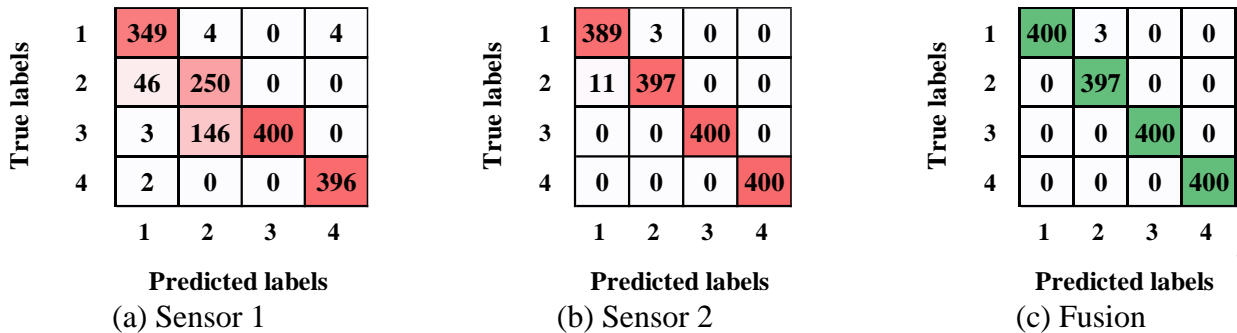


Figure 10 Confusion matrix of diagnosis results

355 Figure 10 presents that the diagnosis result of sensor 1 has a very high false alarm rate for detecting

356 cage fault, thus only 1 weight is given to sensor 1 for voting. In order to combine the excellent
 357 performance in distinguishing cage fault, 2 weights are given to sensor 2 for voting to reduce the false
 358 alarm. Therefore, there is little false alarm rate in the diagnosis result of the fusion.

359 The generalization of the proposed MSCNN-BiLSTM model for multisensory are examined through
 360 the damage evolution scenario, which is compared with the diagnosis results of multisensory information
 361 fused respectively on feature-level and majority voting decision-level. Figure 11

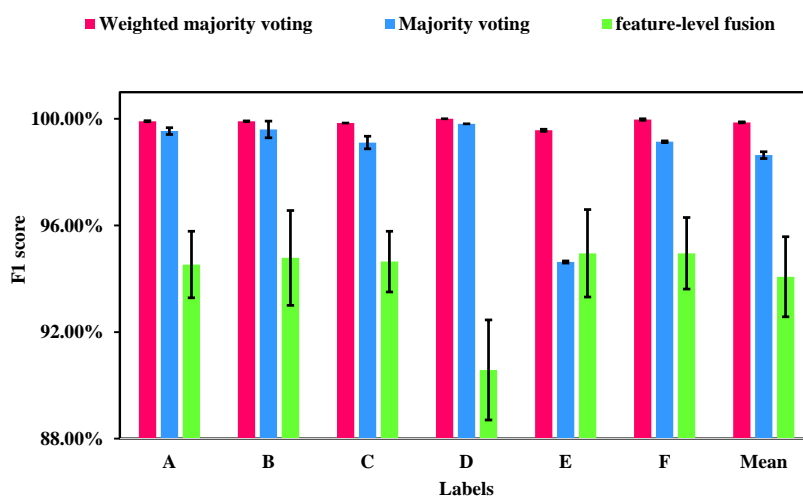


Figure 11: Comparison of the fusion methods for multisensory

362 As shown in Figure 11, the MSCNN-BiLSTM model fused the multisensory information on decision
 363 level through the proposed weighted majority voting rule has a better performance than the other methods
 364 when the examined under damage evolution scenario tests. The mean of F1 scores the weighted majority
 365 voting rule is higher than feature-level fusion for multisensory information by 5.7% and is higher than
 366 traditional majority voting by 1.23%. That indicates that the proposed weighted majority voting rule is
 367 effective.

368 **4.4 Real wind turbine fault diagnosis for multisensory**

369 In real industrial engineering, the model for multisensory diagnosis is offline trained in advanced.
 370 Thus, the data of NREL wind turbine respectively acquired on different days. In the NREL dataset, the

371 data acquired on day 1 is used to train the MSCNN-BiLSTM model, and test the model respectively
 372 through day 2 and day 3. Confusion matrix and the F1 score are used to demonstrate the superiority of
 373 the MSCNN-BiLSTM and to explain the mechanism of the weights majority voting. Table 10 give the
 374 weights of majority voting and the F1 score of each sensor.

Table 10: The weights of majority voting and F1 score for every conditions and sensor

	Weights for majority voting [Sensor1, Sensor2]	F1 Score (Sensor 1/ Sensor 2/ Fusion)
Healthy condition 1	[1, 2]	1.000/1.000/ 1.000
Healthy condition 2	[1, 2]	1.000/1.000/ 1.000
downwind bearing overheating	[1, 2]	1.000/0.9913/ 1.000
downwind bearings damage	[1, 1]	0.9963/0.9622/ 1.000

375 As shown in Table 10, there are some false alarm rate in the case of only using a sensor to diagnosis.
 376 The faults of downwind bearing overheating and damage sometime are misclassified due to a sensor can
 377 not capture useful information for fault diagnosis. The proposed weighted majority voting rule can
 378 integrate the diagnosis results from multiple sensors for improving the performance of the diagnosis. The
 379 sensor 2 takes up a weight 2 votes for healthy condition1, healthy condition2 and bearing overheating,
 380 which can deal with some false alarm rate existed between the condition of bearing overheating and
 381 damage. To further demonstrate the performance of the proposed weighted majority voting, the diagnosis
 382 results of the single sensor and multisensory are respectively presented by confusion matrix in Figure 11.

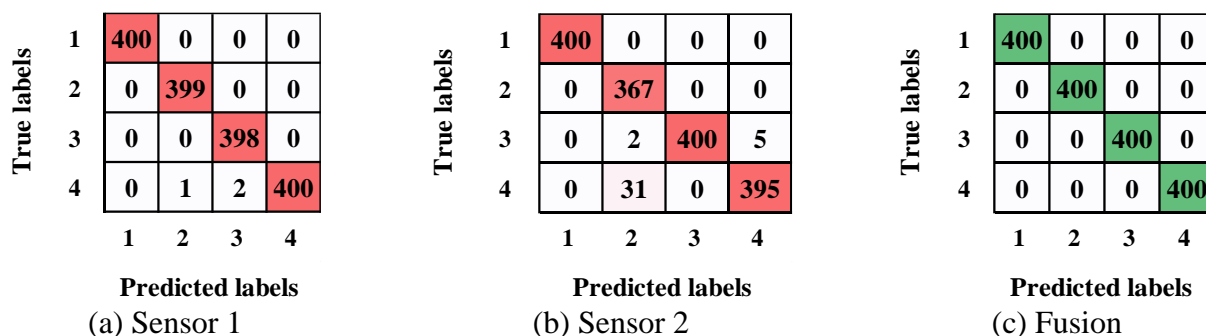


Figure 12 Confusion matrix of diagnosis results

383 As shown in Figure 12, the proposed weighted majority voting rule reduce the false alarm rate
 384 existing between the healthy condition 2 and bearing damage. The mechanism of the weighted majority
 385 voting rule is that Sensor 2 is given more vote weight to health condition 1, health condition 2 and bearing

386 overheating fault to compensate for the bias of diagnosis results on bearing damage. It can be seen that
387 although there are false positives in both sensor 1 and sensor 2 during diagnosis, these false alarms are
388 eliminated after weight voting, which proves the reliability of the proposed method in real wind turbine
389 engineering.

390 **5. Conclusions**

391 A novel fault diagnosis method of wind turbine bearings is developed based on multi-scale coarse-
392 grained procedure algorithm, CNN, BiLSTM and a proposed weighted majority voting rule for
393 multisensory fault diagnosis. The method is combined with the advantages of the CNN in auto features
394 extraction and BiLSTM in capturing the correlation features. CNN is used to extract useful advanced
395 features from the multi-scale sub-signals that generated by an improved multi-scale coarse-grained
396 procedure algorithm, which also can reduce the dimension of the fault features to decrease the calculated
397 amounts of the LSTM unit. In addition, a weighted majority voting rule is designed to fuse the
398 multisensory information in the decision-fusion, which improves the robustness of the MSCNN-BiLSTM
399 model. The verification of our method are examined through multiple groups of experimental data and
400 the main conclusions of this study are as follows:

401 (1) The robustness of the MSCNN-BiLSTM model can be improved by using bidirectional LSTM
402 network to capture forward and backward semantic information between advanced fault features, which
403 has higher diagnosis performance than MSCNN-GRU and MSCNN-LSTM when they are examined in
404 noisy environment.

405 (2) Compared with existing fault diagnosis model developed based on CNN network, the proposed
406 MSCNN-BiLSTM model has the highest F1 score by 97.12% examined through anti-noise test. The
407 generalization of the proposed MSCNN-BiLSTM model is better than the generalizations of the LSTM,

408 the CNN-LSTM, TICNN, MC-CNN, C-CNN, MA-CNN, MCCNN-LSTM and MS-CNN.

409 (3) The proposed weighted majority voting rule can take advantages of a good fault diagnosis results
410 of each sensor to improve the final diagnosis performance. In the damage evolution test scenario, the
411 0.8503 F1 score of the outer race fault, diagnosed by a sensor, is improved by the proposed weighted
412 majority voting rule to increase to 1.0000, which is helped by giving another sensor more vote weights.

413 (4) The proposed weighted majority voting rule is compared with different methods for multisensory
414 diagnosis, that include a traditional majority voting rule that belongs to fusion on decision-level and fusion
415 on feature-level. The results indicate that the proposed weighted majority voting rule is higher than the
416 others by 1.23% and 5.7%.

417 **Acknowledgements**

418 The authors would like to acknowledge the financial support from the National Natural Science
419 Foundation of China (grant numbers: 51676131, 51875361 and 51976131). Shanghai Pujiang Program
420 (2019PJD054). Science and Technology Commission of Shanghai Municipality (grant number:
421 1906052200), Royal Society (grant number: IEC\NSFC\170054), the National Renewable Energy
422 Laboratory and the United States Department of Energy for providing the benchmarking datasets of wind
423 turbine gearbox vibration condition monitoring.

424 **References**

-
- [1] Mbungu, Nsilulu T , et al. "Optimisation of grid connected hybrid photovoltaic–wind–battery system using model predictive control design." *Iet Renewable Power Generation* 11.14(2017):1760-1768.
- [2] Chen, J. , et al. "Generator bearing fault diagnosis for wind turbine via empirical wavelet transform using measured vibration signals - ScienceDirect." *Renewable Energy* 89(2016):80-92.
- [3] Teng, W. , et al. "Compound faults diagnosis and analysis for a wind turbine gearbox via a novel vibration model and empirical wavelet transform." *Renewable Energy* 136.JUN.(2019):393-402.
- [4] Xu, Z. , C. Li , and Y. Yang . "Fault diagnosis of rolling bearing of wind turbines based on the

Variational Mode Decomposition and Deep Convolutional Neural Networks." *Applied Soft Computing* 95(2020):106515.

[5] Xu, Z. , C. Li , and Y. Yang . "Fault diagnosis of rolling bearings using an Improved Multi-Scale Convolutional Neural Network with Feature Attention mechanism." *ISA Transactions* (2020).

[6] Li, B. , et al. "Application of Artificial Neural Networks to photovoltaic fault detection and diagnosis: A review." *Renewable and Sustainable Energy Reviews* 138(2020):110512.

[7] Jing, L. , et al. "An Adaptive Multi-Sensor Data Fusion Method Based on Deep Convolutional Neural Networks for Fault Diagnosis of Planetary Gearbox." *Sensors (Switzerland)* 17.2(2017):414.

[8] Cao, L. , et al. "Fault Diagnosis of Wind Turbine Gearbox Based on Deep Bi-Directional Long Short-Term Memory Under Time-Varying Non-Stationary Operating Conditions." *IEEE Access* 7(2019):1-1.

[9] Wang, Z. , J. Wang , and Y. Wang . "An intelligent diagnosis scheme based on generative adversarial learning deep neural networks and its application to planetary gearbox fault pattern recognition." *Neurocomputing* 310.OCT.8(2018):213-222.

[10] Wang, Tianyang , et al. "Vibration based condition monitoring and fault diagnosis of wind turbine planetary gearbox: A review." *Mechanical Systems and Signal Processing* 126.JUL.1(2019):662-685.

[11] H Zuo, et al. "Effects of different poses and wind speeds on wind-induced vibration characteristics of a dish solar concentrator system." *Renewable Energy* 168(2021).

[12] Huang, Y. , M. Gu , and M. Naggar . "Effect of soil-structure interaction on wind-induced responses of supertall buildings with large pile groups." *Engineering Structures* 243.2(2021):112557.

[13] Wang, J. , et al. "A multi-scale convolution neural network for featureless fault diagnosis." 2016 International Symposium on Flexible Automation (ISFA) IEEE, 2016.

[14] Chen, Z. , K. Gryllias , and W. Li . "Mechanical fault diagnosis using Convolutional Neural Networks and Extreme Learning Machine." *Mechanical Systems and Signal Processing* 133(2019).

[15] Jiang, et al. "Multiscale Convolutional Neural Networks for Fault Diagnosis of Wind Turbine Gearbox." *IEEE Transactions on Industrial Electronics* (2019).

[16] Zhao, B. , et al. "Intelligent fault diagnosis of rolling bearings based on normalized CNN considering data imbalance and variable working conditions." *Knowledge-Based Systems* 199(2020):105971.

[17] X Wang, D. Mao , and X Li. "Bearing fault diagnosis based on vibro-acoustic data fusion and 1D-CNN network." *Measurement* 173.6(2021):108518.

[18] Zhang, W., et al. "A deep convolutional neural network with new training methods for bearing fault diagnosis under noisy environment and different working load." *Mechanical systems and signal processing*(2018):439-453.

[19] Huang, W. , et al. "An improved deep convolutional neural network with multi-scale information for bearing fault diagnosis." *Neurocomputing* 359(2019):77-92.

[20] Zhao R. , Yan, J R, Wang, K. Mao, Learning to monitor machine health with convolutional bi-directional lstm networks, *Sensors* 17 (2) (2017) 273.

[21] Lu, W. , et al. "Early Fault Detection Approach With Deep Architectures." *IEEE Transactions on Instrumentation and Measurement* (2018):1-11.

[22] Jing, L. , et al. "An Adaptive Multi-Sensor Data Fusion Method Based on Deep Convolutional Neural Networks for Fault Diagnosis of Planetary Gearbox." *Sensors (Switzerland)* 17.2(2017):414.

[23] Ma, A , et al. "Multisensor data fusion for gearbox fault diagnosis using 2-D convolutional neural network and motor current signature analysis." *Mechanical Systems and Signal Processing* 144.

[24] Chen, Z. , and W. Li . "Multisensor Feature Fusion for Bearing Fault Diagnosis Using Sparse Autoencoder and Deep Belief Network." *IEEE Transactions on Instrumentation and Measurement* (2017):1-10.

[25] Liu, J. , et al. "An integrated multi-sensor fusion-based deep feature learning approach for rotating

-
- machinery diagnosis." *Measurement Science & Technology* (2018).
- [26]Shao, H. , et al. "A novel approach of multisensory fusion to collaborative fault diagnosis in maintenance." *Information Fusion* (2021).
- [27]Hochreiter, S. , & Schmidhuber, J. (1997). Long short-term memory. *Neural Computation*, 9 (8), 1735-1780.
- [28]Lin, Z. , et al. "Coordinated pitch & torque control of large-scale wind turbine based on Pareto efficiency analysis." *Energy* 147.MAR.15(2018):812-825.
- [29]Wang, Z. , H. Huang , and Y. Wang . "Fault diagnosis of planetary gearbox using multi-criteria feature selection and heterogeneous ensemble learning classification." *Measurement* 173.5(2020):108654.
- [30]Huang, R. , et al. "Deep Ensemble Capsule Network for Intelligent Compound Fault Diagnosis Using Multisensory Data." *IEEE Transactions on Instrumentation and Measurement* 69.5(2020):2304-2314.
- [31]Zwickl, D. J. . "Genetic algorithm approaches for the phylogenetic analysis of large biological sequence datasets under the maximum likelihood criterion." *Dissertations & Theses - Gradworks* 3.5(2008):257-260.
- [32]Wade, et al. "Rolling element bearing diagnostics using the Case Western Reserve University data: A benchmark study." *Mechanical Systems and Signal Processing* 64-65(2015):100-131.
- [33]Wang, B. , et al. "A Hybrid Prognostics Approach for Estimating Remaining Useful Life of Rolling Element Bearings." *IEEE Transactions on Reliability* (2018):1-12.
- [34]Sheng, S. . "Report on Wind Turbine Subsystem Reliability - A Survey of Various Databases (Presentation)." *Office of Scientific & Technical Information Technical Reports* (2013).
- [35]Sheng. "Investigation of Various Condition Monitoring Techniques Based on a Damaged Wind Turbine Gearbox." (2011).
- [36]Ma, X. , and E. Hovy . "End-to-end Sequence Labeling via Bi-directional LSTM-CNNs-CRF." (2016).
- [37]Gal, Y. , & Ghahramani, Z. . (2015). A theoretically grounded application of dropout in recurrent neural networks. *Stats*, 285-290.
- [38]Lei, J. , Liu, C. , & Jiang, D. . (2019). Fault diagnosis of wind turbine based on long short-term memory networks. *Renewable Energy*, 133(APR.), 422-432.
- [39]Hao, S. , et al. "Multisensor Bearing Fault Diagnosis Based on One-dimensional Convolutional Long Short-Term Memory Networks." *Measurement* 159(2020):107802.
- [40]Zhang,W., et al. "A deep convolutional neural network with new training methods for bearing fault diagnosis under noisy environment and different working load. " *Mech Syst Signal Process* (2018):439–453.
- [41]Chang, Y. , et al. "Intelligent fault diagnosis of Wind Turbines via a Deep Learning Network Using Parallel Convolution Layers with Multi-Scale Kernels." *Renewable Energy* 153(2020).
- [42]Wang, H. , et al. "Intelligent Bearing Fault Diagnosis Using Multi-Head Attention-Based CNN." *Procedia Manufacturing* 49(2020):112-118.
- [43]Chen, X. et al. "Bearing fault diagnosis base on multi-scale CNN and LSTM model." *Journal of Intelligent Manufacturing* 32(2021).